PARAMETRIC FINITE ELEMENT ANALYSIS OF PUNCHING SHEAR BEHAVIOUR OF RC SLABS REINFORCED WITH BOLTS

M. Navarro[1], S. Ivorra[1,2,*], F. B. Varona[1]

[1] *Department of Civil Engineering, University of Alicante. San Vicente Del Raspeig, Apartado 99, 03080, Spain*

[2] *Department of Civil Engineering, University of Bristol, Queen's Building, University Walk, Clifton, Bristol, BS8 1TR, United Kingdom.*

ABSTRACT

Reinforced concrete slabs are an essential part of high-rise structures and are designed to withstand the loads to which they are subjected. However, concrete slabs may fail due to punching shear, which is one of the greatest risks they face. This type of failure, hard to predict, befalls almost instantaneously and may lead to catastrophic consequences. In this paper, we analyse a series of non-linear numerical models ─using ABAQUS─ simulating the punching shear effect on a flat, reinforced concrete slab retrofitted with bolts arranged in three different positions around the support. As starting point, we carried out an initial calibration of the Finite Element Model (FEM) using Adetifa and Polak's experimental results. We then performed a parametric analysis to determine the influence of the geometrical parameters of the retrofitting. For this purpose, we created over two hundred models with the help of an automation algorithm programmed in Python. Our results effectively predict the precise distribution of the retrofitting bolts that will successfully increase the punching shear strength.

KEYWORDS

Flat slab, reinforced concrete, bolts, nonlinearity, FEM analysis, parametric study, automatization, structural retrofit.

1 Introduction

In concrete slabs punching shear failures occur in a brittle manner─ abruptly and without any warning. Therefore, in most of the cases, the consequences of these failures tend to be tragic [1], [2]. Fernández-Ruiz et al [3] refer to a case in which a fire breaking out in a parking building caused the failure of a reinforced concrete (RC) slab next to a support due to punching shear. This RC slab failure triggered the complete collapse of the whole frame, and the death of seven firemen. Fernández-Ruiz et al. also reported the presence of other factors intervening in the collapse, these being: (i) an unexpected load located on the roof, (ii) the lack of transverse reinforcement that limited the final deformation significantly, and (iii) poor calculations, which underestimated the punching shear phenomenon. In the field of safety, resistance to punching

* Corresponding author. Tel.: +34 965903400 x 1119; fax: Fax: +34 96 590 3678. E-mail address: sivorra@ua.es (S. Ivorra), Salvador.Ivorra@bristol.ac.uk (S. Ivorra)

shear is arguably the most critical feature in a conventional flat or waffle RC slab building structure, and so the problem needs to be examined carefully.

The phenomenon of punching shear has been studied for a number of years in a number of studies, numerical [4] and experimental [5], [6]. De Borst and Nauta [7], Cervera et al. [8] and Shehata and Regan [9] may be said to be pioneers in applying FEM to describe the phenomenon of punching shear failure. In the 1990s, Marzouk and Hussein [6] and Lips et al. [10] described the behaviour of concrete slabs experimentally, focusing on the different mechanical and geometrical parameters affecting punching shear failures. Menétrey et al. [11] simulated how cracks impacted on the failure mode. In the late 1990s and early 2000s, Polak and Genikomsou [12]–[14] developed FEM models to simulate the experimental results in punching shear tests on RC slabs accurately.

Concrete plastic damage has recently been studied by Wosatko et al. [15]. They have proposed and compared two theories: Gradient-enhanced damage plasticity and Rate-dependent damage plasticity. In the former, they contend that the evolution of the gradient makes the constitutive model to be non-local. In the latter, they introduce a parameter associated with the viscoelastic deformation. Shu et al. [19] have examined the influence of the fracture energy and shear retention. Cavagnis et al. [16], on their part, have used photogrammetry to tackle failure evolution.

Analytical models have also been proposed to assess punching shear strength, those by Menétrey [17], Muttoni [18], and Marí et al. [19] are worth mentioning.

Studies have also been carried out on slabs subjected to other different conditions: Micallef et al. [20] analysed numerically the dynamic impact on a RC slab, and Almeida et al. [21], the reverse horizontal loading and the vertical load to which RC slabs may be subjected.

Comparatively, not much research has focused on how punching shear failure is affected by parameters such as (i) reinforcement type, (ii) reinforcement configuration and external reinforcement for retrofitting, and (iii) reinforcement geometrical and mechanical ratios. Menétrey et al. [11] produced one of the first studies in this area. They focused on parameters, such as concrete strength, amount of reinforcement, and geometric relationships applied to an axisymmetrical model on a circular column. Later, he [17] published a synthesis of RC slab failure, delivering experimental results and numerical simulations from which he derived an analytical model. Guan [22] centred his study in the size and location of the cracks in relation to on the column. Belletti et al. [23] compared the numerical predictions –based on a non-linear finite element made up of two-dimensional reinforcing layers– with the experimental results and analytical values obtained from the application of different standards.

Still other authors have compared their experimental and analytical results with different analytical model regulation specifications. Inácio et al. [24], for example, contend that the main regulations might overestimate the strength of the slab, especially for high values, and Navarro et al. [25] present a parametric analysis of RC slabs without retrofitting and compare some predictions with Eurocode 2 [26] and Model Code 2010 [27].

Now, the types of reinforcement with which a slab can be retrofitted are varied. They include steel or fibre reinforced polymer (FRP) plates or strips, different configurations of external shear bolts (acting as additional transverse reinforcement), and variations in concrete composition. El-Salakawy et al. [28] studied the effect of slab openings in the column's neighbourhood and the carbon/glass-fibre external reinforcement strips.

Durucan and Anil [29] carried out a similar study. Polak and others [30]–[32] illustrated, both experimentally and numerically, the effects of steel and FRP shear bolts used as transverse reinforcement on punching shear failure. Meisami et al. [33] also proposed reinforcement alternatives to RC slabs. These consist in carbon fibre reinforced polymer (CFRP) grids and bolts fixed with epoxy resins in obliquely drilled holes effected from the bottom of the slab. Pilakoutas and Li [34] presented an undulating-steel-band type of reinforcement. Dam and Wight [35] and Elbarkry and Allam [36] highlight the effectiveness of different bolt layouts in rails and plates.

Still other reinforcement types need especial mention. They are those that modify the concrete composition not only by altering the basic components and using (i) lightweight aggregates [37], (ii) lightweight cement [38], but also by placing concrete with high compressive strength in the centre of the floor [39]. Other solutions contemplate the incorporation of FRP [40]–[43], and steel fibres [43] to CR slabs.

This article focuses on the analysis of the influence of the aforementioned factors. This parametric analysis is carried out using slab models developed in ABAQUS, taking advantage of the available models for plastic damage of concrete [44]–[46]. Numerical simulations have proven to help reduce costs in terms of experimental studies of RC failure mechanisms [47], [48], thus facilitating further parametric research and proposals as well as the incorporation of different formulation and behaviour models.

After the introduction, in the second section, we will show that Adetifa and Polak's test results [49] on a RC slab retrofitted with shear bolts will serve us to calibrate the FEM model numerically. In the third section, we will make a comparison between the experimental data and the numerical results to help us validate the main features of the FEM model itself. In the fourth section, we will apply the numerically calibrated FEM model to a parametric study of the shear bolt diameter, the number of bolts needed in each configuration, the distance between the first shear bolt and the face of the column, the spacing of the subsequent shear bolts, and the geometrical layout of the bolt placement. The combination of these parameters has provided us with 243 different models, which can be automated when programmed in Python [50] for ABAQUS [46] to reduce labour time. In the fifth section, we draw the most relevant conclusions and propose further lines of research. One of them we suggest is to devise a reliable modelling tool to assess the real capacity of the reinforcement in both one-way and waffle slabs so as to design the reinforcement, e.g. using FRP, precisely ─see Meisami et al [33] and Faria et al. [51].

The novelty of this article resides in two main aspects: a) the development of a parametric study centred on the retrofitting of a RC flat slab –in a non-linear three-dimensional FEM model–, and b) the innovative character of the code creation and automation of FEM models.

2 Description of the experimental background

For the calibration of the FEM model, we used Adetifa and Polak's [49] test results. These results are drawn from real-scale models of RC slabs to column connections. The slabs measure 1800×1800×120 mm, and the column studs, protruding from both the upper and lower faces of the slab, have a height of 150 mm and a cross section of 150×150 mm. Table 1 shows the concrete mechanical properties, steel reinforcing bars, and external reinforcement shear bolts–required to reproduce Adetifa and Polak's test results from which we calibrate our FEM model.

Table 1. Material properties of the slab tested in [49]

Compressive strength of concrete [MPa]	**Tensile strength of concrete [MPa]**	**Yield strength of steel reinforcement [MPa]**	**Yield strength of steel shear bolts [MPa]**
41	2.1	455	381

The longitudinal flat slab reinforcement consists of a top and bottom 10M-bar mesh of 100 mm^2 in cross-sectional area. These bars are located on the compression and tension zones. Those in the compression zone are 200 mm apart in both X and Y orthogonal directions while the bars located in the tension zone are spaced 100 mm in both directions. The concrete layer covering the longitudinal bar centre is 20 mm thick. As for the column stud reinforcement, it consists of four 20M longitudinal bars of 300 mm^2 in cross-sectional area, and four 8M confinement bars acting as shear reinforcement having a cross-sectional area of 50 mm^2. The column studs have an effective depth of 130 mm. For boundary conditions, the slab is simply supported along the edges on small neoprene supports, creating spans of 1500 mm in the X and Y directions.

The external transverse reinforcement shear bolts were fitted in 16 mm diameter holes, drilled around the column studs prior to testing. Depending on the number of shear bolts, we devised and tested several specimens. However, only the test results from specimen SB4 are going to be used for calibration. The configuration of specimen SB4 shows the placement of the shear bolts to be concentric and parallel to the perimeter of the column. Each row of shear bolts has two bolts parallel to the face of the column stud. Specimen SB4 has, in fact, four rows of bolts per column face (see Fig. 1b), which means that a total of 32 shear bolts have been fitted.

The load keeps being transmitted through the column studs until the failure point is reached, and failure occurs in a brittle manner due to punching shear. (Note that the experimental layout is opposite to that of a real structure because it test). Fig. 1b shows the shape of the crack at failure point, and Fig. 1a the crack pattern in specimen SB1 –equal to SB4 but lacking the external shear bolts and consequently, transverse reinforcement. The relationship between the applied load and the vertical displacement of the centre of the lower face of the column was recorded. Table 4 and Fig. 5 show load-displacement response.

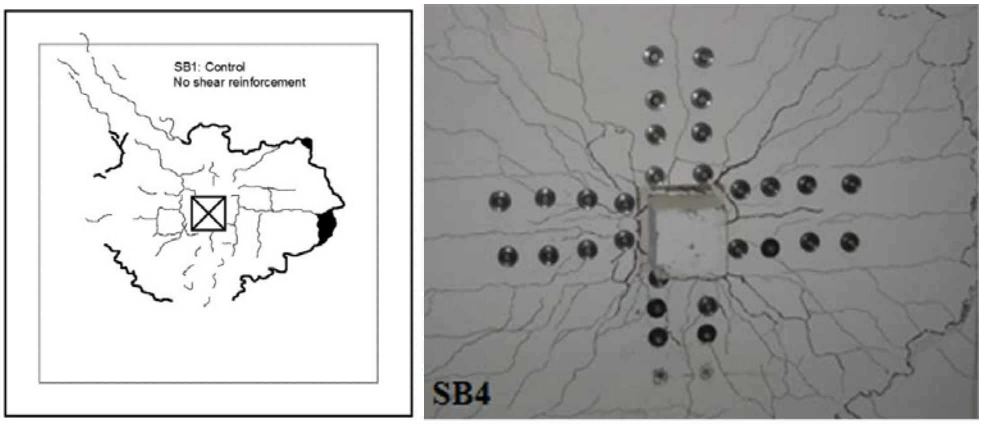

Fig. 1. Crack pattern from experimental study [49]: (a) test carried out in a specimen without shear bolts as transverse reinforcement; (b) test carried out in specimen SB4, with 32 shear bolts.

3 Implementation of the slab numerical model

3.1 Features of the model

The FEM has been implemented in ABAQUS [46] for calibration. The program is capable of simulating accurately the non-linearity of materials, such as steel and concrete and besides, it has been applied by Mirza [52], Obaidat [53] and Alfarah et al. [54] to simulate concrete structures successfully. Now, for experimental purposes and because of the symmetry in the load and in geometry of the entire column, we have modelled just one quarter of the slab-column connection to reproduce Adetifa and Polak's experimental tests [49]. Then, this quarter of the slab shows simple supports on its two outer edges and the corresponding symmetry conditions have been applied to its inner edges. The test carried out with a vertical displacement control gradually increases linearly over time. See Fig. 2 and Fig. 3 for details.

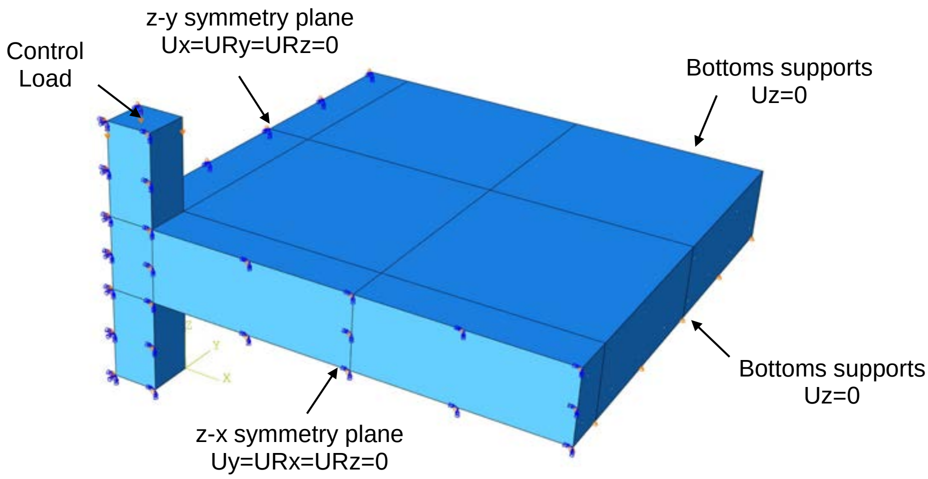

Fig. 2. Geometry and boundary conditions of the model.

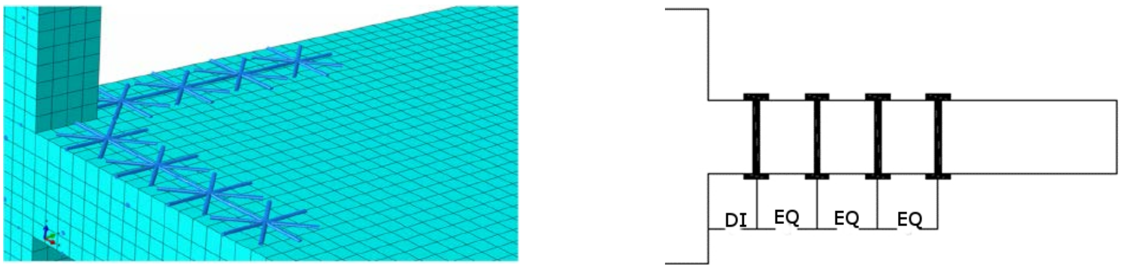

Fig. 3. Shear bolt disposition in the slab model simulating specimen SB4 in [49]. Left: general view of the FEM. Right: scheme showing location and spacing of shear bolts.

For the purpose of studying the behaviour of concrete, we have applied the Concrete Damage Plasticity model, available in ABAQUS. In this context, concrete is said to display two types of failure mechanisms: cracking and crushing. The model is a revision of Drucker and Prager's approach [55], which, in turn, assumes Lubliner et al.'s criterion [45] and incorporates Lee and Fenves' adjustments [44] to address the evolution of both compression strength and tension strength in concrete. Since the main stresses appear in various directions, the tension-strain relationship can be defined through Eq. (1).

$$\sigma=(1-d)D_0^{el}:(\varepsilon-\varepsilon^{pl}) \quad (1)$$

where d is the scalar stiffness degradation variable, whose values range from zero (undamaged) to one (completely damaged); D_0^{el} the initial elasticity matrix; ε the total strain; and ε^{pl} the plastic deformation.

The constitutive behaviour of concrete in compression is based on the Model Code CEB 2010 [27] and is represented in Fig. 4a, where σ_c is the compression stress, ε_c the deformation of concrete, f_{cm} the average compression strength of concrete, $\varepsilon_{c,lim}$ the ultimate strain, E_{cm} the tangent modulus of elasticity and E_{c1} the secant modulus of elasticity. With regard to the concrete uniaxial behaviour in tension, its constitutive model is based on Hillerborg et al.'s fracture energy

[56] –Fig. 4b and Fig. 4c– where σ_t is the tensile stress, ε_c the concrete strain, w the crack width, and G_f the fracture energy.

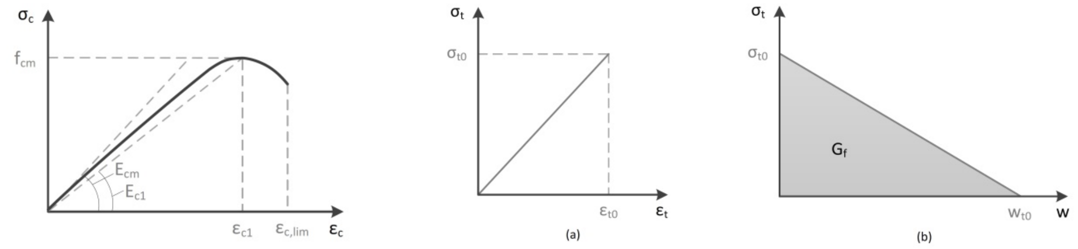

(a) (b) (c)

Fig. 4. Constitutive behaviour of concrete: (a) in compression, in compliance with Model Code 2010 [27]; (b) in tension before cracking; (c) softening after cracking, according to Hillerborg et al. [57].

For steel reinforcement, we have adopted the bi-linear model proposed in Eurocode 2 [26]. Starting with a linear elastic curve, the model reaches the steel yield strength f_y and then a second curve follows up to the point the model fails at a stress equal to f_s, a higher point than that of the yield strength. In addition, we have applied the Von Misses failure criterion to steel. The bolts are assumed to be perfectly elastic as they never reach tensions close to their yield strength. Also, the surfaces of concrete and steel are assumed to be perfectly bonded, a common practice in the study of reinforced concrete pieces globally analysed (Genikomsou and Polak [13], and Wosatko et al. [58]).

The concrete mesh has been made up of 8-node hexahedral elements with reduced integration (C3D8R), the longitudinal reinforcement meshes within the RC slab of 4-node reduced-integration shell elements (S4R), the reinforcement bars in the concrete studs protruding the RC slab of 2-node truss elements with reduced integration (T3D2), and finally, the shear bolts of 3-node quadratic beams in space (B32).

In line with the experimental test, we use a displacement control method in the FEM slab model. We set a constant vertical displacement speed for the application of the vertical load. Thus, the convergence problems that would entail a load-control solution are minimized.

Table 2 shows the observed calibrated values taken from the Concrete Damage Plasticity model to tally Adetifa and Polak's [49] experimental results. Table 3 exhibits the calibrated values for the behaviour of concrete subjected to compression and to tension.

Table 2. Calibrated values for the *Concrete Damage Plasticity* finite element analysis (FEA).

	Dilation angle ψ	**Excentricity ε**	**Viscosity μ**	**Shape parameter K_c**	**Max. compression axial/biaxial**
Genikomsou & Polak [59]	40°	0.1	0	1.16	0.667
Current FEA	36º	0.1	0.00001	1.16	0.667

Table 3. Concrete properties associated with the constitutive behaviour of concrete in compression and in tension.

	Modulus of elasticity of concrete [MPa]	**Poisson's ratio**	**Fracture energy of concrete [N/mm]**	**Tensile strength of concrete [MPa]**
Genikomsou & Polak [59]	35217	0.2	0.077	2.2
Current FEA	35217	0.2	0.105	2.1

3.2 Validation of the calibration for the slab model

Fig. 5 and Table 4 show the experimental results from [49], and the load displacement responses from our calibrated finite element analysis (FEA). Fig. 5 illustrates the SB1 (specimen without shear reinforcement) load deflection curve, the SB4 (specimen with shear reinforcement) load deflection curve, our FEA results, and Genikomsou and Polak's FEA results [13]. The values of the parameters of [13] can be found in Tables 2 and 3. These tables show slight differences in general terms. However, note that in Genikomsou and Polak's FEM model, the slab longitudinal reinforcement consisting of T3D2 elements to represent each of the bars has been replaced in our analysis by a continuous mesh already introduced in the previous section.

Figure 5 shows that for displacements greater than 10 mm and loads in excess of 250 kN, the calibrated FEA results offer a better agreement with the experimental results than that proposed in [13], which can be readily appreciated in the 25-30 mm interval, just before failure. Our calibrated model overestimates both the stiffness of the slab-column connection for small displacements and small loads (in the range of 50 to 125kN) Table 4 illustrates the level of concordance between our model and Adetifa and Polak's experiment results: the relative error of ultimate load and ultimate displacement are 0.28% and 1.01%, respectively.

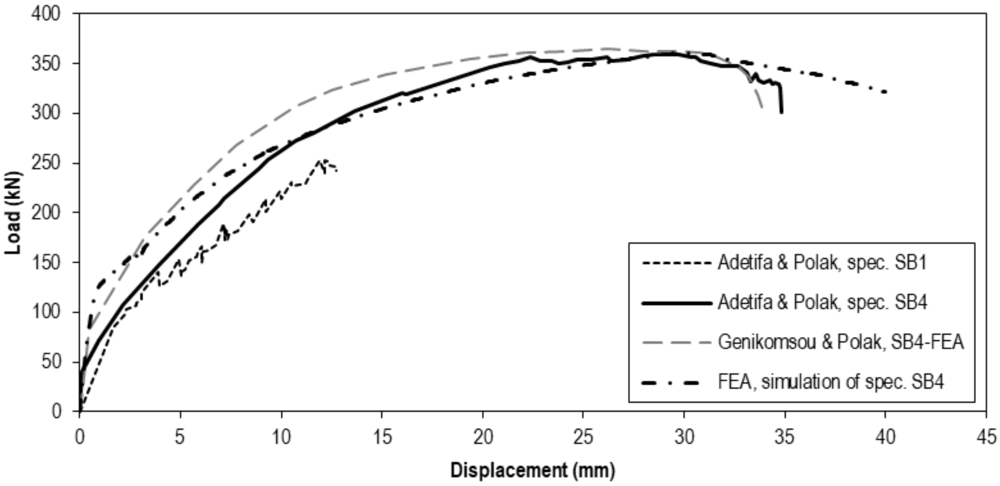

Fig. 5. Load–deflection responses obtained in the tests by Adetifa and Polak [49], in the FEA by Genikomsou and Polak [59] and in the current FEA with the calibrated parameters.

Table 4. Results of punching shear tests reported in [49] and through FEA of the calibrated numerical model for RC slab with shear bolts.

Without shear reinforcement		**With shear reinforcement**			
Adetifa and Polak [49], **specimen SB1**		**Adetifa and Polak** [49], **specimen SB4**		**Current FEA with calibrated parameters**	
Ultimate load (kN)	Ultimate deflection (mm)	Ultimate load (kN)	Ultimate deflection (mm)	Ultimate load (kN)	Ultimate deflection (mm)
253	11.9	360	29.8	361	30.1

3.3 Parametric analysis variables

Table 5 shows our source model for a parametric study. It will be compared with other models exhibiting different reinforcement configurations. The variables taken into account are: diameter of the bolts, number of bolts in each layout, distance from the first bolt to the face of the support; (DI), spacing between bolts, (EQ), and layout of the shear bolts. Table 6 illustrates the three different values or types assigned to each variable.

Table 5. Values of parameters in the reference model for parametric study.

Variable	**Initial value**
Yield strength of steel (MPa)	500
Concrete compresive strength (MPa)	25
Longitudinal reinforcement ratio	1.5%
Column width/Slab width ratio	0.1
Column width/Slab thickness ratio	1.25
Punching shear reinforcement	None

Table 6. Values adopted for each variable

Parámetro	**Value 1**	**Value 2**	**Value 3**
Bolts diameter (mm)	Ø8	Ø12	Ø16
Number of bolt pairs per support face	2	3	4
First bolt-column distance (mm)	3.5·Ø	5·Ø	6.5·Ø
Distance between bolts (mm)	5·Ø	6.5·Ø	8·Ø
Bolt disposition	Double line	Radial	Diamond

The range of values taken for DI, the first-bolt to column distance, and for EQ, bolt spacing is in conformity with Eurocode 2 [26] and EHE-08 [60].

We have devised 243 models which make up all possible combinations of the 5 parameters over 3 values. The main features of the chosen parameters are that distances DI and BQ are a function of the diameter selected, which has an effect on the final geometrical layout. Identical geometry and number of bolts but different reinforcement diameters will affect the area covered by the retrofitting.

Every model was subjected to FEA with control displacement at constant vertical speed. The displacement was applied at the same point in each model and showed a maximum vertical deflection of 40 mm. We observed that a vertical deflection of 20 mm was insufficient to reach the failure point in most of the cases. Figure 6 illustrates the different bolt layouts. All 243 models were programmed in Python and solved in ABAQUS. The two most relevant data ─ultimate load and its associated ultimate displacement─ are shown in Tables 7 and 8.

3.4 Automating parametrization analyses

Structural engineering and engineering in general need to be competent in computer techniques to develop their projects [61], [62]. In the field of materials properties simulation, their skills are oriented towards the parameterization of the models' features, both at the level of materials and geometric shape and at automating processes. The latter proves critical in reducing time involved in creating FEM models, obvious in our present study. Programming in Python [50] has made automation possible. It enables to program a code to control the processes step by step in ABAQUS to produce FEM models in every phase ─parameterization and automation, analysis, and data collection [63].

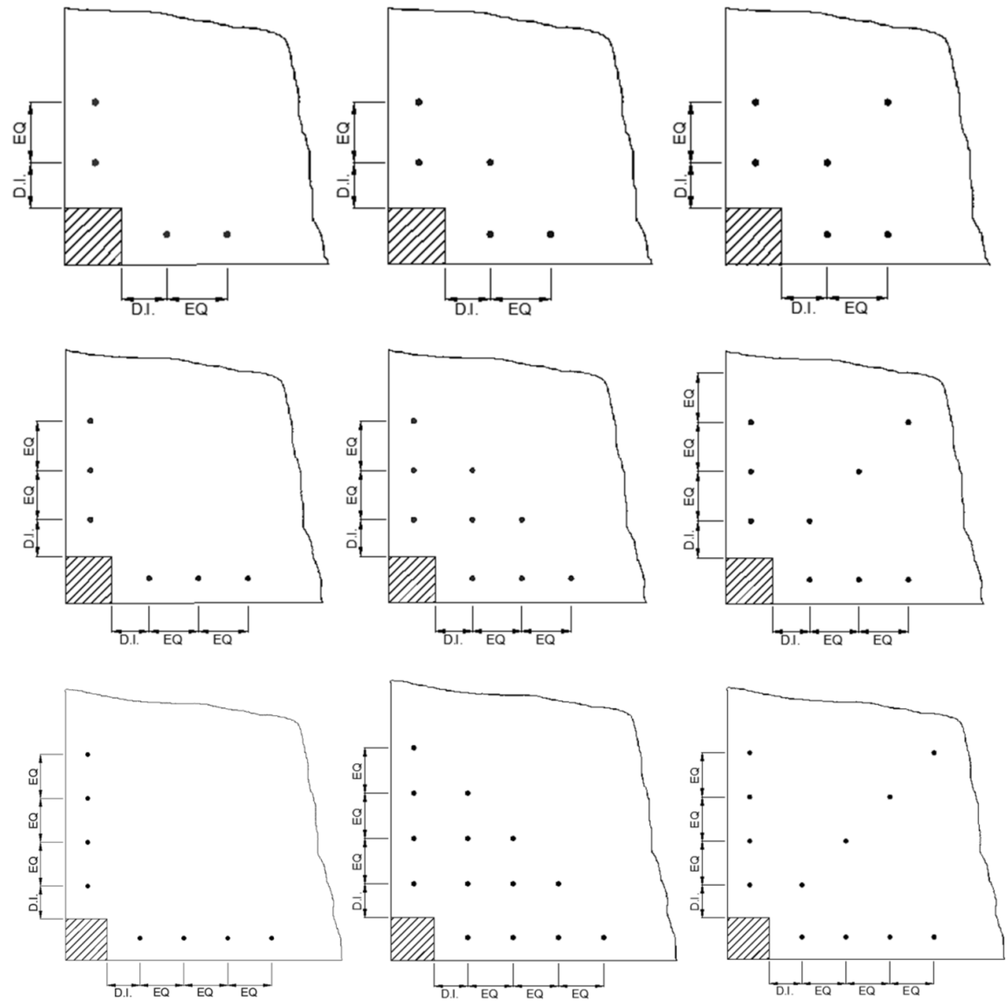

Fig. 6. Bolts disposition: 2 bolts (upper row), 3 bolts (middle row), 4 bolts (bottom row); double line disposition (left column), radial disposition (middle column), diamond disposition (right column).

We find two ways to automate the process and save execution time. In the first, the model is calculated when the previous one has ended. In the second, the model is structured in batches. Moreover, we can select the range and parameterization intervals to offer greater usability. Useful as this selection may be, it poses the problem of computational overload, especially in the second option since the limit, dictated by the user, must not exceed the processing capabilities of the computer.

ABAQUS [46] has an immense library of commands written in Python [63] crucial for the development of the code model and its parameterization and automation presented in this paper. Among the commands, a user interface has been designed to significantly increase comfort and the intuitive nature of the parameterization and automation performed.

4 Analysis of the results

4.1 Introduction

An Intel Core i7 340 GHZ processor made the calculations in 4 hours per model in average. Since the number of FEM models analysed rules out the possibility of including our results in this paper, we present a selection of the most remarkable findings in our experiments. Therefore, we show the ultimate load for each of the 243 models in Table 7, and their ultimate deflection in Table 8. It is worth mentioning that some designs with radial and diamond layouts with bolts 16 mm in diameter reached a vertical deflection of 40 mm –the displacement control limit– before failing. Thus, no conclusive data could be taken out from them. Table 7 and Table 8 present the results multi-dimensionally, illustrating the interrelation among the 5 parameters above mentioned. The nine columns take into consideration the diameter of the shear bolts and the number of pairs of bolts per support face. The rows, on the other hand, are grouped in terms of geometrical configuration, distance *EQ* (bolt spacing), and distance *DI* (between the first bolt to the support's face).

We also make use of a coloured scale. In Table 7, the lowest values of the ultimate load are in green whilst the highest values of the load are in red. Thus, it is readily seen that the most effective retrofit layout for shear bolts is the diamond configuration with 4 pairs of bolts 12 mm in diameter per support face (see Fig. 6, bottom row, right column, and a total of 48 bolts).

As ductility is associated with the ultimate displacement, Table 8 shows that the diamond configuration with shear bolts 12 mm in diameter does not seem to be the most suitable layout for punching shear retrofit despite having the highest value of ultimate load. The radial configuration with 4 pairs of bolts 12 mm in diameter per support face corresponds to a middle level –moderate ductility and a remarkable increase in the value of ultimate load. Especially noteworthy is the design in which (*DI*) is 5·Ø (60 mm) and (*EQ*) is 6.5·Ø (78 mm) because it yields an ultimate load of almost 400 kN and an ultimate displacement in excess of 30 mm.

Table 7. Ultimate load depending on the geometrical disposition of shear bolts, distances *EQ* and *DI*, diameter of bolts and number of pairs of bolts per support face.

			Ultimate load (kN)								
			Diameter ∅8 mm Pairs of bolts			Diameter ∅12 mm Pairs of bolts			Diameter ∅16 mm Pairs of bolts		
	EQ	*DI*	2	3	4	2	3	4	2	3	4
DOUBLE LINE	5·∅	3.5·∅	333.9	347.8	366.8	339.2	370.3	393.5	325.9	328.5	326.4
		5·∅	329.5	357.9	362.8	316.0	323.1	320.4	314.8	316.5	318.0
		6.5·∅	333.9	319.9	327.9	312.7	313.5	314.2	312.7	311.1	308.5
	6.5·∅	3.5·∅	333.0	356.1	375.1	360.2	391.4	398.5	326.3	325.7	320.6
		5·∅	335.6	355.5	367.8	317.8	322.3	322.2	314.9	317.0	317.6
		6.5·∅	360.2	325.9	313.7	321.2	319.5	319.6	315.8	314.6	313.9
	8·∅	3.5·∅	342.7	361.2	388.8	365.6	390.4	395.2	329.2	322.4	323.2
		5·∅	340.4	363.8	368.8	316.5	317.1	317.4	317.7	315.4	315.7
		6.5·∅	319.9	324.5	326.4	318.7	317.8	317.0	314.4	312.2	315.5
RADIAL	5·∅	3.5·∅	342.5	381.8	379.6	378.4	415.3	460.7	402.3	428.2	460.3
		5·∅	358.8	379.5	399.9	377.8	395.7	407.3	324.3	340.2	337.2
		6.5·∅	361.2	386.4	407.2	371.8	378.4	382.9	316.4	327.5	329.1
	6.5·∅	3.5·∅	360.4	389.5	402.5	385.3	418.4	449.4	371.3	395.2	333.5
		5·∅	365.7	387.1	427.2	382.4	385.0	398.6	322.6	344.9	341.4
		6.5·∅	360.6	383.9	386.7	367.4	371.2	379.6	323.3	341.8	381.8
	8·∅	3.5·∅	362.2	386.2	418.0	380.8	416.5	446.5	370.2	375.4	380.7
		5·∅	365.3	404.6	418.7	370.8	372.1	390.3	341.6	348.5	348.5
		6.5·∅	362.4	362.4	383.8	367.6	363.5	377.3	329.8	328.0	343.0
DIAMOND	5·∅	3.5·∅	337.7	365.4	389.9	357.0	393.9	429.7	380.8	396.7	413.8
		5·∅	334.8	375.2	398.5	358.9	410.7	453.3	324.9	351.5	356.8
		6.5·∅	346.9	378.5	407.7	350.8	406.2	455.3	328.9	344.6	352.6
	6.5·∅	3.5·∅	342.7	389.5	405.7	367.5	406.8	460.0	372.5	379.0	385.6
		5·∅	346.4	378.0	405.4	382.4	421.6	484.5	328.0	349.8	353.4
		6.5·∅	337.1	383.1	417.4	348.6	400.2	457.0	330.2	336.5	344.2
	8·∅	3.5·∅	347.3	379.8	413.6	375.0	427.5	496.2	363.2	374.9	376.0
		5·∅	354.4	386.9	420.3	362.1	417.4	476.2	332.0	339.4	344.4
		6.5·∅	343.5	390.1	399.3	353.0	408.0	433.2	319.6	335.4	343.4
			Lowest		←	Ultimate load			→		Highest

Table 8. Ultimate displacement (associated to ultimate load), depending on the geometrical disposition of shear bolts, distances *EQ* and *DI*, diameter of bolts and number of pairs of bolts per support face.

			Ultimate displacement (mm)								
			Diameter ∅8 mm Pairs of bolts			Diameter ∅12 mm Pairs of bolts			Diameter ∅16 mm Pairs of bolts		
	EQ	*DI*	2	3	4	2	3	4	2	3	4
DOUBLE LINE	5·∅	3.5·∅	27.65	23.01	22.98	21.04	23.87	27.84	28.90	31.27	28.26
		5·∅	25.91	29.22	28.30	28.21	29.21	28.06	28.11	31.35	27.78
		6.5·∅	27.65	28.56	30.17	27.32	27.04	28.05	28.31	27.86	30.07
	6.5·∅	3.5·∅	22.97	21.78	23.28	25.98	29.63	29.13	30.58	28.88	26.85
		5·∅	26.98	27.90	29.34	28.91	30.62	29.48	28.08	32.53	28.86
		6.5·∅	25.98	31.23	32.21	30.95	29.37	30.33	33.43	31.37	28.51
	8·∅	3.5·∅	26.33	22.34	22.98	27.06	30.51	30.29	31.07	33.17	32.09
		5·∅	26.34	29.57	28.50	28.17	27.68	28.00	32.91	33.84	32.34
		6.5·∅	28.98	30.14	29.10	31.54	29.73	29.40	28.29	29.51	32.23
RADIAL	5·∅	3.5·∅	19.84	22.79	20.98	20.83	19.73	20.63	26.36	29.51	33.13
		5·∅	23.88	22.53	21.09	26.63	26.46	27.61	31.16	40.00	32.22
		6.5·∅	25.40	26.08	28.11	28.09	26.64	26.72	31.38	34.05	30.09
	6.5·∅	3.5·∅	24.52	22.34	18.61	22.03	22.74	25.70	27.89	40.00	33.03
		5·∅	24.28	23.14	22.45	28.87	28.02	32.30	28.78	40.00	36.00
		6.5·∅	26.02	27.55	26.31	28.85	30.25	31.52	33.99	40.00	40.00
	8·∅	3.5·∅	22.02	23.22	21.59	24.65	25.64	28.81	28.22	33.72	40.00
		5·∅	24.28	25.26	23.90	30.54	30.22	34.97	40.00	40.00	40.00
		6.5·∅	27.31	25.55	28.54	32.70	29.97	33.87	40.00	40.00	40.00
DIAMOND	5·∅	3.5·∅	23.35	20.61	19.10	22.26	17.55	15.17	24.70	29.29	27.29
		5·∅	20.35	21.68	19.11	27.17	24.79	21.33	29.78	40.00	36.68
		6.5·∅	26.99	23.72	21.09	27.09	27.62	25.84	40.00	40.00	40.00
	6.5·∅	3.5·∅	23.34	21.47	17.90	22.06	17.72	19.10	30.59	35.18	27.74
		5·∅	23.24	20.17	17.20	28.87	25.79	23.34	35.70	40.00	34.89
		6.5·∅	25.38	24.16	22.17	28.80	26.48	26.35	40.00	40.00	37.27
	8·∅	3.5·∅	23.43	18.87	16.30	23.67	20.07	19.73	26.37	30.22	27.34
		5·∅	26.73	20.30	19.18	27.17	25.69	25.05	36.16	40.00	40.00
		6.5·∅	27.16	26.73	30.21	27.61	28.37	25.29	30.05	40.00	40.00
			Highest		←	Ultimate displacement		→			Lowest

4.2 Effect of the shear bolt diameter on the retrofit

Regarding the ultimate load, we have observed that an increase in diameter from 8 mm to 12 mm produced an increase in the ultimate load by an average of 3.3%. However, if the diameter increased from 12 mm to 16 mm, the ultimate load decreased by 10% in average. This behaviour was particularly noticeable in the diamond configuration, in which the load increased by 9% when the diameter changed from 8 mm to 12 mm, but the load decreased by 13.8% when the diameter went from 12 mm to 16 mm. Fig. 7a illustrates a double line geometry layout and shows the effect the diameter has on a retrofitting design. This layout exhibits 3 pairs of bolts per support face, *DI* = 5·Ø and *EQ* = 8·Ø. The reason for the unexpected decrease in the ultimate load ─diameter increasing from 12 mm to 16 mm─ can be found in the distances DI and EQ. They increase alongside the diameter and, consequently, the area affected by the shear bolts falls beyond the critical perimeter. As a result, a relatively low number of 16 mm bolts effectively controlled the punching shear failure. Fig. 7b illustrates the effect of switching bolts of 8 mm to 12 mm in the diamond layout. In this case, the layout exhibited 2 pairs of bolts and distances *DI* = 5·Ø and *EQ* = 6.5·Ø. We can appreciate that the average ultimate load was reduced. We find, again, that the diameters of the bolts are the reason for the results obtained and, what is more, we believe that a decrease in ultimate load occurs with bolts of greater diameters because of a lower density of shear bolts per area.

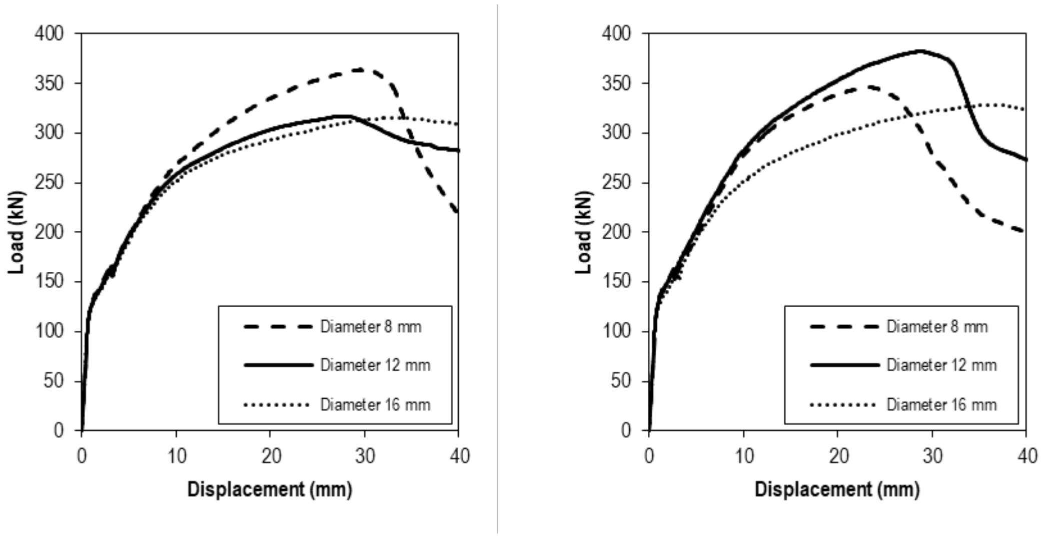

(a) (b)

Fig. 7. Selected examples of load-deflection FEA results: (a) double line layout, 3 pairs of shear bolts, *DI* = 5·Ø and *EQ* = 8·Ø; (b) diamond layout, 2 pairs of shear bolts, *DI* = 5·Ø and *EQ* = 6.5·Ø.

In terms of ductility, we observed that as the diameter of the shear bolts increased from 8 mm to 12 mm, the displacement also increased by an average of 9.4%. However, when the diameter increased from 12 mm to 16 mm, the displacement increased by an average of 25.1%. Nonetheless, there were some cases in the double line geometry in which the increase in diameter from 8 mm to 12 mm produced a decrease in ductility (see Fig. 7b). An increase in ductility is much more noticeable in radial layout ─15%─ for the same diameters. If the bolt diameters switched from 12 mm to 16 mm, the diamond geometry proved to be the most sensitive to ductility increase ─44.5%.

4.3 Effect of the number of bolts on the retrofit

In terms of the ultimate load, an increase in the number of pairs of bolts per support face –from 2 to 3– brought about an average increase of 5.6% in the ultimate load. Moreover, if the number increased from 3 to 4 pairs, the ultimate load increased 4.1% in average. The diamond geometry was found most affected by this variable: an increase of 9.6% for switching from 2 to 3, and 7.2% from 3 to 4 pairs. In contrast, the double line geometry proved less affected in that the ultimate load increased less than 2%. Figures 8 and 8a show a double line layout for shear bolts of 8 mm and for shear bolts of 16 mm in diameter, respectively. In the latter configuration, a larger diameter implied longer *DI* and *EQ* distances, resulting in their being beyond the critical perimeter, and so the addition of more bolts affected neither the ultimate load nor the ductility variables (see Figure 8b). For the same reason, the effect of the number of 16 mm bolts on the radial and diamond configurations was less than 4.1% (2 to 3 pairs) and less than 2% (3 to 4 pairs).

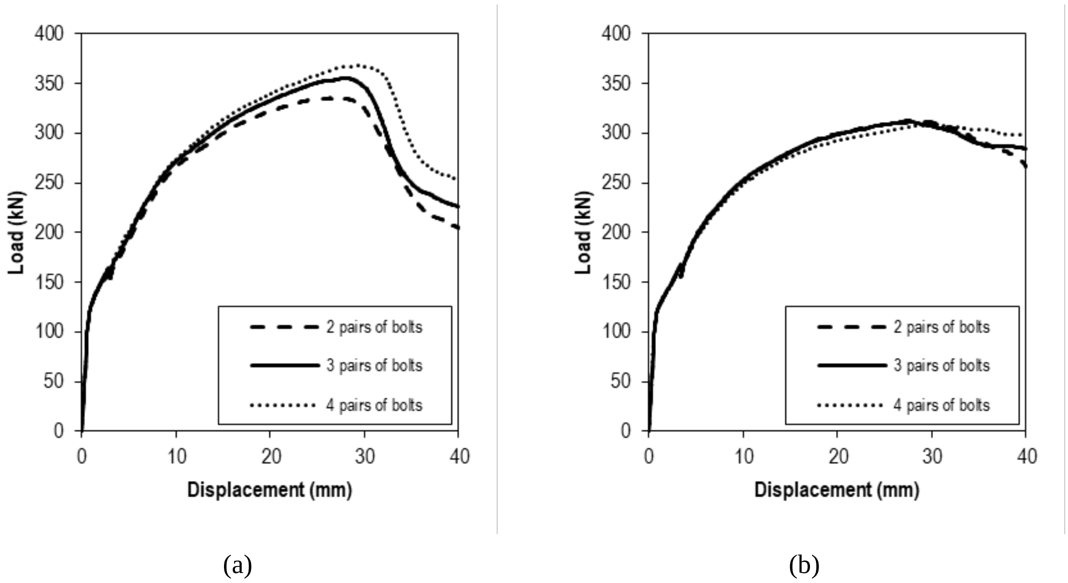

Fig. 8. Load-deflection response with shear bolts placed in double line layout: (a) 8 mm diameter bolts, *DI* = 5·Ø and *EQ* = 6.5·Ø; (b) 16 mm diameter bolts, *DI* = 6.5·Ø and *EQ* = 5·Ø.

We observed that the radial layout exhibited the largest increase in the ultimate displacement when the pair of bolts per support face rose from 2 to 3 ─ a negligible reduction of 0.2% was recorded for the diamond configuration. Neither in the double line layout nor in the radial geometry did we find any significant increase in the ultimate deflection ─less than 1%─ if we switched from 2 to 3 pairs of bolts. However, we did observe a reduction in ultimate deflection of 6.9% in the diamond configuration. We assume that the reason lies in this typology having the highest density of bolts per area, which reduces ductility in favour of strength.

4.4 Effect of the distance from the first bolt to the column on the retrofit

We observed that the distance between the first bolt pair and the column (*DI*) matters. If increased from 3.5·Ø to 5·Ø, the models' ultimate load decreased by an average of 5.1%. Double line and radial layouts showed a reduction of approximately 6 and 7%, respectively. In the diamond configuration the load was less affected, less than 3%. If on the other hand, (*DI*) increased from 5·Ø to 6.5·Ø, the ultimate load decreased by an average of 2.5%. Fig. 9 presents the general trends associated with the models exhibiting a radial geometry with 4 pairs of bolts 12 mm in diameter per face, and a spacing *EQ* = 6.5·Ø. As previously seen, a high value of the initial distance (*DI*) moves the bolts away from the column and consequently, fewer bolts lie within the critical perimeter.

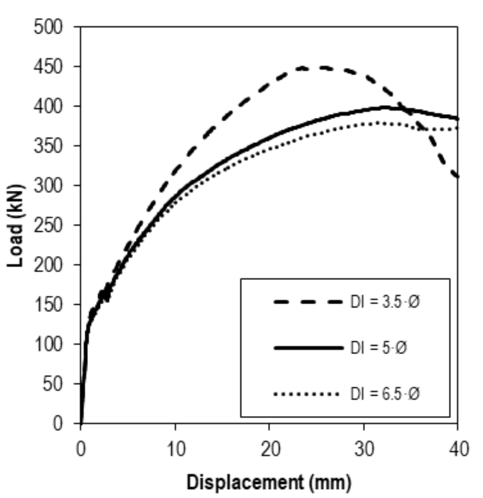

Fig. 9. Load-deflection response of the FEM model with radial disposition, 4 pairs of bolts per support face, 12 mm diameter bolts and *EQ* = 6.5·Ø.

Conversely, if the distance *DI* increased, ductility also increased. When *DI* increased from 3.5·Ø to 5·Ø, so did the ultimate displacement: 7.7% for double line, 15.2% for radial, and 20.9% for diamond. However, if *DI* increased from 5·Ø to 6.5·Ø, the ductility increased 1.4% in the double line layout and 9.1% in the diamond geometry.

4.5 Effect of the spacing between bolts on the retrofit

In double line and diamond layouts, spacing *EQ* had the same effect on the ultimate load. If *EQ* increased from 5·Ø to 6.5·Ø, the ultimate load also increased by approximately 1.2%; and a further *EQ* increase from 6.5·Ø to 8·Ø yielded no change in the load. However, in the radial geometry, an increase in *EQ* produced a decrease in the load of about 1%. Fig. 10 shows a model in diamond configuration with 2 pairs of bolts per support face, bolts 8 mm in diameter, and distance *DI* = 6.5·Ø

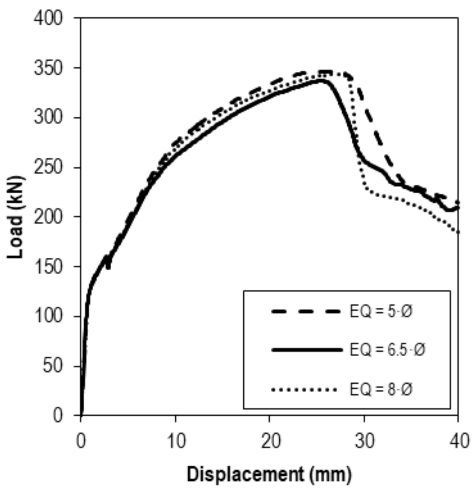

Fig. 10. Load-deflection response of the FEM model with diamond layout, 2 pairs of shear bolts per support face, 8 mm diameter bolts and *DI* = 6.5·Ø.

Spacing *EQ* also affects the ultimate displacement but not equally in all layouts. In the radial layout, we observed that when *EQ* changed from 5·Ø to 6.5·Ø, the ultimate displacement increased as much as 8.8%. Moreover, if *EQ* =8·Ø, the displacement increased by 6.3%. The other layouts were less responsive: the increase amounted to less than 3.9%.

4.6 Effect of the shear bolt layout on the retrofit

In this section, we compare the standard double line, radial and diamond configurations in terms of bolts layout. Radial and diamond geometries were more effective than double line in upholding the ultimate load by FEM models. In radial and diamond configurations, the increase in ultimate load with reference to double line was 12.7% and 13.9%, respectively. Fig. 11 shows load-deflection curves through FEA from models with 3 pairs of 8 mm bolts (Fig. 11a) and with 4 pairs of 16 mm bolts (Fig. 11b). In terms of number of pairs of bolts, we observed that (i) with 2 pairs of bolts per support face, radial proved more effective than double line: its ultimate load increased 9.6% greater; (ii) when 3 pairs of bolts were involved, radial and diamond behaved equally effective and better than double line, showing an increase in ultimate load of 13.5% (see Fig. 11a); (iii) with 4 pairs of bolts per support face, diamond provided the best response: 20.9% in average greater than double line (see Fig. 11b).

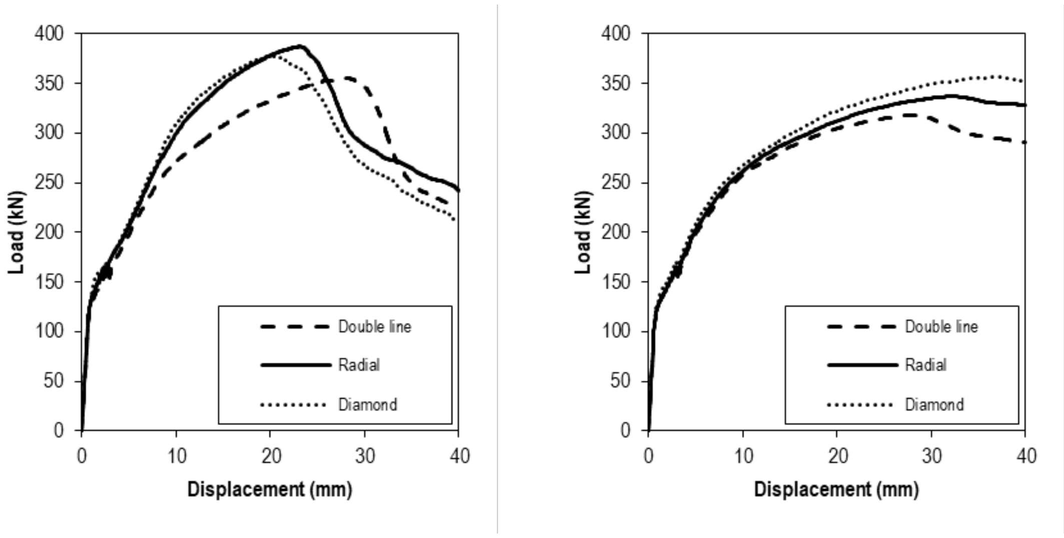

(a) (b)

Fig. 11. Load-deflection response of the FEM models: (a) 3 pairs of shear bolts of Ø8 mm per support face, *DI* = 5·Ø and *EQ* = 6.5·Ø; (b) 4 pairs of bolts of ∅16 mm, *DI* = 5·Ø and *EQ* = 6.5·Ø.

Conversely, diamond provided the poorest response for punching shear ductility compared to double line; diamond showed an average loss of 1.3% –2 pairs of bolts per support face– and of 10.3% –4 pairs. Fig. 11a illustrates this trend. Nonetheless, Fig. 11b provides us with an exceptional instance in which diamond showed greater ductility. As for radial, also compared to double line, ductility was seen to decrease by 1.2% with 2 pairs of bolts but to increase by an average of 1.8% to 3.1% with 3 and 4 pairs of bolts, respectively.

5. Conclusions

The use of RC flat slabs retrofitted with bolts to avoid punching shear has been studied by means of FEM models implemented in ABAQUS. The FEM model was calibrated quantitatively and qualitatively to match the experimental and numerical results offered in scientific literature concerning the topic. We have also applied the Concrete Damage Plasticity model.

The FEM model has also allowed us to develop a parametric analysis to study the effects of the different variables on the RC structural response of retrofitted flat slabs against punching shear.

As the spacing between shear bolts is likely to be proportional to the diameter of the bolts, identical geometry and number of bolts of different diameter will have a particular effect on the area under the influence of the retrofitting.

The main conclusions related to the parametric study are the following:

- An increase in bolt diameter will trigger an increase in ultimate displacement and a decrease in ultimate load. Bolts 16 mm in diameter may be the reason for some of them falling beyond the critical perimeter area, causing, at the same time, a significant loss in strength.

- An increase in number of bolts in any layout generally produces an increase in ultimate load. However, if 16 mm bolts are used, the increase in ultimate load is less significant in radial and diamond, and even detrimental in double line. We find that the explanation, again, lies in the number of bolts existing within the critical perimeter: diamond is more densely reinforced –and, thus less affected. The addition of a third pair of bolts per support face increased ductility. Surprisingly, the addition of a fourth pair caused a decrease in ductility, especially in diamond.
- Taking the spacing between the column and the first bolt pair (*DI*) into consideration, the models that exhibited greater ultimate load were those whose *DI* was 5·Ø. When *DI* = 3.5· Ø, the model falls short of reaching the critical perimeter, and when DI = 6.5· Ø, it goes beyond. But as far as ductility is concerned, it decreases when *DI* increases, the reason probably being the insufficient concentration of transverse reinforcement around the column.
- The spacing between bolts (*EQ*) seems not to be as decisive as *DI* for calculating ultimate load. Variations in ductility can be explained in terms of variations in *DI*.
- Radial and diamond have more pairs of bolts than double line. Diamond has the greatest density within the critical perimeter of the column. Therefore, when *DI* decreases, the critical perimeter is denser and ductility decreases. Furthermore, with *DI* = 5·Ø, the greatest ultimate load is reached, validating our previous conclusions. In terms of ductility, diamond showed the greatest loss in ductility. All in all, radial responded the best since it provided an adequate increase in ultimate load without compromising ductility, and it even showed a slight gain in ductility for a higher number of shear bolts.
- Although code management in ABAQUS can be complex for its requirements of combined skills and knowledge of Civil Engineering and Computer Engineering, it has been essential in the development of our models, especially the parametric ones. Even though code programming is time-consuming, it has allowed us to automate processes, saving a great deal of time in the creation of many of our models.

As a final remark, we firmly believe that the results obtained have paved the way towards future work aimed at systematically finding the optimum design parameters.

6. Acknowledgements

The authors wish to express their gartitude to the Technical University of Valencia for sharing ABAQUS with us. A special mention needs to be made to Dr. Vicente Albero and Dr. David Pons for their assistance and advice in the application of the capabilities of this software.

7. References

[1] J. Kunz, M. Fernández-Ruiz, and A. Muttoni, *Enhanced safety with post-installed punching shear reinforcement*, no. l. London: Taylor & Francis Group, 2008.

[2] D. Foti, “Shear vulnerability of historical reinforced-concrete structures,” *Int. J. Archit. Herit.*, vol. 9, no. 4, pp. 453–467, May 2015.

[3] M. Fernández-Ruiz, A. Muttoni, and J. Kunz, “Strengthening of flat slabs against punching shear using post-installed shear reinforcement,” *ACI Struct. J.*, vol. 107, no. 4, pp. 434–442, 2010.

[4] D. Jiang and J. Shen, “Strength of Concrete Slabs in Punching Shear,” *J. Struct. Eng.*, vol. 112, no. 12, pp. 2578–2591, 1986.

[5] Ronaldo B. Gomes and P. E. Regan, “Punching Resistance of RC Flat Slabs with Shear Reinforcement,” *J. Struct. Eng.*, vol. 125, no. 6, pp. 684–692, 1999.

[6] H. Marzouk and A. Hussein, “Experimental investigation on the behavior of high-strength concrete slabs,” *ACI Structural Journal*, vol. 88, no. 6. pp. 701–713, 1991.

[7] R. de Borst and P. Nauta, “Non-orthogonal cracks in a smeared finite element model,” *Eng. Comput.*, vol. 2, no. 1, pp. 35–46, 1985.

[8] M. Cervera, E. Hinton, and O. Hassan, “Nonlinear analysis of reinforced concrete plate and shell structures using 20-noded isoparametric brick elements,” *Comput. Struct.*, vol. 25, no. 6, pp. 845–869, Jan. 1987.

[9] I. A. E. M. Shehata and P. E. Regan, “Punching in R.C. slabs,” *J. Struct. Eng.*, vol. 115, no. 7, pp. 1726–1740, Jul. 1989.

[10] S. Lips, M. Fernández-Ruiz, and A. Muttoni, “Experimental investigation on punching strength and deformation capacity of shear-reinforced slabs,” *ACI Struct. J.*, vol. 109, no. 6, pp. 889–900, 2012.

[11] P. Menétrey, R. Walther, T. Zimmermann, K. J. Willam, and P. E. Regan, “Simulation of punching failure in reinforced-concrete structures,” *J. Struct. Eng.*, vol. 123, no. 5, pp. 652–659, 1997.

[12] M. A. Polak, “Modeling punching shear of reinforced concrete slabs using layered finite elements,” *ACI Struct. J.*, vol. 95, no. 1, pp. 71–80, 1998.

[13] A. S. Genikomsou and M. A. Polak, “Finite element analysis of a reinforced concrete slab-column connection using ABAQUS,” in *Structures Congress 2014*, 2014, pp. 813–823.

[14] A. Genikomsou and M. A. Polak, “Damaged plasticity modelling of concrete in finite element analysis of reinforced concrete slabs,” in *Proceedings of the 9th International Conference on Fracture Mechanics of Concrete and Concrete Structures*, 2016.

[15] A. Wosatko, J. Pamin, and M. A. Polak, “Application of damage–plasticity models in finite element analysis of punching shear,” *Comput. Struct.*, vol. 151, pp. 73–85, 2015.

[16] F. Cavagnis, M. Fernández Ruiz, and A. Muttoni, “Shear failures in reinforced concrete members without transverse reinforcement: An analysis of the critical shear crack development on the basis of test results,” *Eng. Struct.*, vol. 103, pp. 157–173, 2015.

[17] P. Menétrey, “Synthesis of punching failure in reinforced concrete,” *Cem. Concr. Compos.*, vol. 24, no. 6, pp. 497–507, Dec. 2002.

[18] A. Muttoni, “Punching shear strength of reinforced concrete slabs without transverse reinforcement,” *ACI Struct. J.*, vol. 105, no. 4, pp. 440–450, 2008.

[19] A. Marí, A. Cladera, E. Oller, and J. M. Bairán, “A punching shear mechanical model for reinforced concrete flat slabs with and without shear reinforcement,” *Eng. Struct.*, vol. 166, pp. 413–426, 2018.

[20] K. Micallef, J. Sagaseta, M. Fernández Ruiz, and A. Muttoni, “Assessing punching shear failure in reinforced concrete flat slabs subjected to localised impact loading,” *International Journal of Impact Engineering*, vol. 71. pp. 17–33, 2014.

[21] A. F. O. Almeida, M. M. G. Inácio, V. J. G. Lúcio, and A. P. Ramos, “Punching behaviour of RC flat slabs under reversed horizontal cyclic loading,” *Eng. Struct.*, vol. 117, pp. 204–219, 2016.

[22] H. Guan, “Prediction of punching shear failure behaviour of slab-edge column connections with varying opening and column parameters,” *Adv. Struct. Eng.*, vol. 12, no. 1, pp. 19–36, 2009.

[23] B. Belletti, J. C. Walraven, and F. Trapani, “Evaluation of compressive membrane action effects on punching shear resistance of reinforced concrete slabs,” *Eng. Struct.*, vol. 95, pp. 25–39, Jul. 2015.

[24] M. M. G. Inácio, A. F. O. Almeida, D. M. V Faria, V. J. G. Lúcio, and A. P. Ramos, “Punching of high strength concrete flat slabs without shear reinforcement,” *Eng. Struct.*, vol. 103, pp. 275–284, 2015.

[25] M. Navarro, S. Ivorra, and F. B. Varona, “Parametric computational analysis for punching shear in RC slabs,” *Eng. Struct.*, vol. 165, pp. 254–263, Jun. 2018.

[26] European Committee for Standarisation, *Eurocode 2: Design of concrete structures - Part 1-1: General rules and rules for buildings*. Madrid: AENOR, 2013.

[27] International Federation for Structural Concrete (fib), *fib Model Code for Concrete Structures 2010*. Berlin: Ernst & Sohn, 2013.

[28] E. El-Salakawy, K. Soudki, and M. A. Polak, “Punching shear behavior of flat slabs strengthened with fiber reinforced polymer laminates,” *J. Compos. Constr.*, vol. 8, no. 5, pp. 384–392, 2004.

[29] C. Durucan and Ö. Anil, “Effect of opening size and location on the punching shear behavior of interior slab-column connections strengthened with CFRP strips,” *Eng. Struct.*, vol. 105, pp. 22–36, 2015.

[30] M. A. Polak and N. Lawler, “Application of FRP for punching shear retrofit of concrete slab-column connections,” in *Advances in FRP Composites in Civil Engineering - Proceedings of the 5th International Conference on FRP Composites in Civil*

Engineering, CICE 2010, 2011, pp. 854–857.

[31] N. Lawler and M. A. Polak, “Development of FRP shear bolts for punching shear retrofit of reinforced concrete slabs,” *J. Compos. Constr.*, vol. 15, no. 4, pp. 591–601, 2011.

[32] A. S. Genikomsou and M. A. Polak, “Finite element analysis of RC flat slabs with different amount and placement of shear bolts,” in *American Concrete Institute, ACI Special Publication*, 2017, vol. 2017–Janua, no. SP 321, pp. 80–98.

[33] M. H. Meisami, D. Mostofinejad, and H. Nakamura, “Punching shear strengthening of two-way flat slabs with CFRP grids,” *J. Compos. Constr.*, vol. 18, no. 2, p. 04013047, Apr. 2014.

[34] K. Pilakoutas and X. Li, “Alternative shear reinforcement for reinforced concrete flat slabs,” *J. Struct. Eng.*, vol. 129, no. 9, pp. 1164–1172, 2003.

[35] T. X. Dam and J. K. Wight, “Flexurally-triggered punching shear failure of reinforced concrete slab-column connections reinforced with headed shear studs arranged in orthogonal and radial layouts,” *Eng. Struct.*, vol. 110, pp. 258–268, 2016.

[36] H. M. F. Elbakry and S. M. Allam, “Punching strengthen ing of two-way slabs using external steel plates,” *Alexandria Eng. J.*, vol. 54, no. 4, pp. 1207–1218, 2015.

[37] K.-S. Youm, J. J. Kim, and J. Moon, “Punching shear failure of slab with lightweight aggregate concrete (LWAC) and low reinforcement ratio,” *Constr. Build. Mater.*, vol. 65, pp. 92–102, 2014.

[38] J.-B. Yan, J.-Y. Wang, J. Y. Richard Liew, X. Qian, and W. Zhang, “Reinforced ultra-lightweight cement composite flat slabs: Experiments and analysis,” *Mater. Des.*, vol. 95, pp. 148–158, 2016.

[39] P. Zohrevand, X. Yang, X. Jiao, and A. Mirmiran, “Punching shear enhancement of flat slabs with partial use of ultrahigh-performance concrete,” *J. Mater. Civ. Eng.*, vol. 27, no. 9, 2015.

[40] A. M. T. Hassan, G. H. Mahmud, S. W. Jones, and C. Whitford, “A new test method for investigating punching shear strength in Ultra High Performance Fibre Reinforced Concrete (UHPFRC) slabs,” *Compos. Struct.*, vol. 131, pp. 832–841, 2015.

[41] A. W. El-Ghandour, K. Pilakoutas, and P. Waldron, “Punching Shear Behavior of Fiber Reinforced Polymers Reinforced Concrete Flat Slabs: Experimental Study,” *J. Compos. Constr.*, vol. 7, no. 3, pp. 258–265, 2003.

[42] A. Caratelli, S. Imperatore, A. Meda, and Z. Rinaldi, “Punching shear behavior of lightweight fiber reinforced concrete slabs,” *Compos. Part B Eng.*, vol. 99, pp. 257–265, 2016.

[43] K.-H. Tan and P. Paramasivam, “Punching shear strength of steel fiber reinforced concrete slabs,” *J. Mater. Civ. Eng.*, vol. 6, no. 2, pp. 240–253, 1994.

[44] J. Lee and G. L. Fenves, “Plastic-damage model for cyclic loading of concrete

structures," *J. Eng. Mech.*, vol. 124, no. 8, pp. 892–900, 1998.
[45] J. Lubliner, J. Oliver, S. Oller, and E. Oñate, "A plastic-damage model for concrete," *Int. J. Solids Struct.*, vol. 25, no. 3, pp. 299–326, 1989.
[46] *Abaqus Theory Manual (6.14)*. Dassault Systemes, Providence, RI, USA, 2014.
[47] M. Navarro-Menargues, F.-B. Varona, D. Bru, and S. Ivorra, "Análisis paramétrico automatizado de losas de hormigón sometidas a punzonamiento," *Dyna*, 2018.
[48] P. A. Calderón, J. M. Adam, S. Ivorra, F. J. Pallarés, and E. Giménez, "Design strength of axially loaded RC columns strengthened by steel caging," *Mater. Des.*, vol. 30, no. 10, pp. 4069–4080, 2009.
[49] B. Adetifa and M. A. Polak, "Retrofit of slab column interior connections using shear bolts," *ACI Struct. J.*, vol. 102, no. 2, pp. 268–274, 2005.
[50] G. Puri, *Python scripts for Abaqus*. Kan Sasana Printer, 2011.
[51] D. M. . Faria, J. Einpaul, A. M. P. Ramos, M. Fernández-Ruiz, and A. Muttoni, "On the efficiency of flat slabs strengthening against punching using externally bonded fibre reinforced polymers," *Constr. Build. Mater.*, vol. 73, pp. 366–377, 2014.
[52] O. Mirza and B. Uy, "Behaviour of headed stud shear connectors for composite steel–concrete beams at elevated temperatures," *J. Constr. Steel Res.*, vol. 65, no. 3, pp. 662–674, Mar. 2009.
[53] Y. T. Obaidat, S. Heyden, and O. Dahlblom, "The effect of CFRP and CFRP/concrete interface models when modelling retrofitted RC beams with FEM," *Compos. Struct.*, vol. 92, no. 6, pp. 1391–1398, 2010.
[54] B. Alfarah, F. López-Almansa, and S. Oller, "New methodology for calculating damage variables evolution in Plastic Damage Model for RC structures," *Eng. Struct.*, vol. 132, pp. 70–86, 2017.
[55] D. C. Drucker and W. Prager, "Soil Mechanics and Plastic Analysis or Limit Design," *Q. Appl. Math.*, vol. 10, no. 2, pp. 157–165, 1952.
[56] A. Hillerborg, M. Modéer, and P. E. Petersson, "Analysis of crack formation and crack growth in concrete by means of fracture mechanics and finite elements," *Cem. Concr. Res.*, vol. 6, no. 6, pp. 773–781, Nov. 1976.
[57] A. Hillerborg, M. Modéer, and P. E. Petersson, "Analysis of crack formation and crack growth in concrete by means of fracture mechanics and finite elements," *Cem. Concr. Res.*, vol. 6, no. 6, pp. 773–781, Nov. 1976.
[58] A. Wosatko, J. Pamin, and M. A. Polak, "Application of damage–plasticity models in finite element analysis of punching shear," *Comput. Struct.*, vol. 151, pp. 73–85, 2015.
[59] A. S. Genikomsou and M. A. Polak, "Finite element analysis of a reinforced concrete slab-column connection using ABAQUS," in *Structures Congress 2014*, 2014, pp. 813–823.

[60] Ministerio de Fomento. Gobierno de España, “Instrucción de Hormigón Estructural (EHE-08),” *Real Decreto 1247/2008. Madrid 18 de Julio de 2008. BOE N*^{o} *203*. pp. 35176–35178, 2008.

[61] V. Albero, A. Espinos, M. L. Romero, A. Hospitaler, G. Bihina, and C. Renaud, “Proposal of a new method in EN1994-1-2 for the fire design of concrete-filled steel tubular columns,” *Eng. Struct.*, vol. 128, pp. 237–255, 2016.

[62] H. Behnam, J. S. Kuang, and B. Samali, “Parametric finite element analysis of RC wide beam-column connections,” *Comput. Struct.*, vol. 205, 2018.

[63] “Python Software Foundation webpage.” [Online]. Available: https://www.python.org/.